DOI: 10.1002/marc.((insert number)) ((or ppap., mabi., macp., mame., mren., mats.))

Communication

Observation of Confinement-induced Self-Poling Effects in Ferroelectric Polymer Nanowires grown by Template Wetting

Richard A. Whiter, Yonatan Calahorra, Canlin Ou and Sohini Kar-Narayan*

_____

R. A. Whiter, Y. Calahorra, C. Ou, Dr S. Kar-Narayan
Department of Materials Science and Metallurgy, University of Cambridge, CB3 0FS, UK
E-mail: sk568@cam.ac.uk

_____

((Ferroelectric polymer nanowires grown using a template-wetting method are shown to achieve an orientated 'self-poled' structure resulting from the confined growth process. Self-poling is highly desirable as it negates the need for high electric fields, mechanical stretching and/or high temperatures typically associated with poling treatments in ferroelectric polymers, as required for piezoelectric and/or pyroelectric applications. Here, we present differential scanning calorimetry, infrared spectroscopy and dielectric permittivity measurements on as-fabricated template-grown polyvinylidene fluoride-trifluoroethylene (P(VDF-TrFE)) nanowires, and quantitatively compare the results with spin-cast films of the same composition that have been electrically poled, both before and after subsequent de-poling temperature treatment. The measurements reveal remarkably similar trends between the physical properties of the as-grown nanowires and the electrically poled film samples, providing insight into the material structure of the 'self-poled' nanowires. In addition, piezo-response force microscopy (PFM) data is presented that allows for unambiguous identification of self-poling in ferroelectric polymer nanostructures, and indicates the suitability of the template-wetting approach in fabricating nanowires that can be used directly for

piezoelectric/pyroelectric applications, without the need for post-deposition poling/processing.))

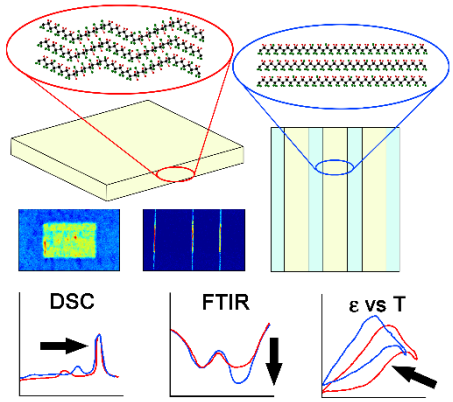

1. Introduction

Organic ferroelectric polymers have recently attracted increasing scientific interest due to a combination of highly desirable material properties and technological advances. Despite exhibiting weaker piezoelectric properties than commonly used ferroelectric ceramics[1] (such as barium titanate and lead zirconium titanate) their piezoelectric properties are still technologically viable[2] while simultaneously possessing a range of advantages over ceramics including being flexible, low-temperature and solution-processable, light weight, non-toxic and biocompatible, chemically robust and mechanically stable.[3] The recent surge in interest has arisen from their suitability in a range of developing technologies such as sensing,[4] actuation[5], non-volatile memory[6-8] and vibrational energy harvesting applications.[2,3] For piezoelectric/pyroelectric applications in particular, there is a requirement for the material to be poled, i.e. to have orientated dipoles, in order for the piezoelectricity/pyroelectricity to manifest. This is typically achieved through externally applied electric fields, high temperatures and/or mechanical stretching.

Polyvinylidene fluoride [PVDF] and its copolymers are by far the most well studied and highest performing piezoelectric polymers. PVDF is semi-crystalline with multiple possible crystalline phases; α, β, γ, δ and ε,[1] of which the all-trans ferroelectric β phase possesses the strongest piezoelectric behaviour.[9] PVDF however readily crystallises in the non-polar α phase which exhibits no piezoelectric behaviour and requires post-deposition poling/ processing to convert it to the β phase or the other crystalline phases of intermediary performance.[10] Due to steric effects, PVDF copolymerised with trifluoroethylene [P(VDF-TrFE)] readily crystallises predominantly into the all-trans β phase[10] over a range of copolymer ratios, making P(VDF-TrFE) desirable in many applications. Unlike PVDF for which no ferroelectric Curie transition is observable, because its melting point precedes when this would otherwise occur,[11,12] Curie transitions are clearly observable in P(VDF-TrFE) with

the Curie temperature depending on the co-polymer ratio, processing conditions and the resulting crystalline properties.[10,13-16]

Nanowires and other nanostructures of PVDF and P(VDF-TrFE) are of particular interest as they have been reported to exhibit enhanced properties including higher ferroelectric crystallinity[17-19,20] higher piezoelectric coefficients[21,22] and lower coercive fields[5,18,19] as well as being capable of being fabricated readily orientated with aligned dipoles without the requirement for further post-fabrication poling processes.[5,17-19,21,23-26] This 'self-poled' nature being intrinsic in the fabrication process is highly advantageous as the large electric fields (~50 MVm^{-1}) and high temperatures otherwise involved in poling may be difficult to achieve in practice.

Electrospinning[4,27], nano-imprinting[6,28] and template-wetting[18,19,21,25,26] fabrication methods have all been reported to produce readily orientated piezoelectric polymers in confined geometries. Template wetting, where the polymer wets and fills a nano-porous template either from the melt or solution, has benefits over the alternative fabrication methods due to its simplicity and the lack of need of specialised equipment, large electric fields and/or high temperatures. Under suitable conditions, the confined geometry results in the polymer self-assembling into an orientated material structure of stacked lamellae to give rise to 'self-poled' nanowires.[18,19,21] This is in contrast with electrospinning where the inherent mechanical stretching and large electric fields involved are believed to be responsible for the resulting orientated material.[27]

Different crystalline geometries have been established for P(VDF-TrFE),[29,30] as shown in Figure 1(a) and 1(b), including (i) the "low-temperature" phase where the polymer chains have all-trans bonds and packing matching that of the β phase with aligned dipoles, and (ii) the "cooled" phase where the bonds are predominantly all-trans but with some gauche bonds causing structural defects where the polymer chains are caused to tilt and small domains are created.[16] Here the consecutively all-trans segments have aligned dipoles but

the dipoles of different segments separated by the gauche defects are not aligned. Electricaly poling P(VDF-TrFE) serves to transform the material from the cooled phase to the low-temperature phase.[30] We have previously shown in Ref [25] that template-grown P(VDF-TrFE) nanowires are indeed self-poled as they are capable of generating a piezoelectric output voltage in response to periodic impacting, without the need of prior electrical poling treatment. Self-poled nanowires of P(VDF-TrFE) implies fabrication directly in the low-temperature phase. Previous studies have shown that upon heating, P(VDF-TrFE) may pass from a ferroelectric crystalline phase to the paraelectric phase in one observable transition or that it may undergo multiple transitions associated with the low-temperature and cooled phases either transforming intermediately from one to the other or separately from each into the paraelectric phase.[15,16] The position in temperature of the transition from ferroelectric to paraelectric phase has also been shown to vary with domain size which can correspond with the extent of gauche defects and therefore also the form of the crystalline stucture.[31]

The nature of the self-poled template-wetted PVDF and P(VDF-TrFE) nanowires is still not fully understood. At the same time, the enhanced piezoelectric properties of these polymer nano-structures, while readily observed, are currently not well explained. While we have previously demonstrated the piezoelectric performance of template-grown self-poled polymer nanowires for applications in energy harvesting [25], in this work we present a detailed comparison of template-wetted P(VDF-TrFE) nanowires with poled and unpoled films of the same composition, using differential scanning calorimetry [DSC], attenuated total internal reflection Fourier transform infrared spectroscopy [ATR-FTIR] and temperature-dependent dielectric permittivity measurements. Our studies clearly show that the template-grown nanowires possess physical characteristics similar to poled films. In addition, piezo-response force microscopy (PFM) measurements taken on the as-grown templated nanowires shine light on their confinement-induced self-poled nature, as compared to as-

grown unpoled films of the same composition where such an effect is found to be absent. The DSC and permittivity measurements were used to establish the ferroelectric Curie temperature for each of the samples studied. Integrals across the peaks in the DSC measurements were used to measure enthalpy changes during the transitions and infer information on overall crystallinity. ATR-FTIR measurements were used to determine the extent of orientation in addition to crystalline structural properties. Vibrational bands such as those occurring at ~840 cm^{-1} and ~880 cm^{-1} are of particular interest. The ~880 cm^{-1} band, which relates to symmetric stretching of CF2 and CC bonds, corresponds to the presence of chains with more than three consecutive trans links and is therefore very sensitive to the ferroelectric crystalline phase, particularly in the low-temperature configuration. The 840 cm^{-1} band, which relates to rocking of CF2 and CH2 bonds as well as anti-symmetric stretching of CF2 bonds, corresponds to any trans links. This therefore means the relative absorption of the ~840 cm^{-1} and ~880 cm^{-1} bands gives an indication of the extent of the all-trans low-temperature crystalline geometry.[32,33]

The two vibrational bands also correspond to different symmetry species with the vibrational transition moment of the ~840 cm^{-1} band being parallel to polar b axis of P(VDF-TrFE) whereas that of the ~880 cm^{-1} band is parallel to the a axis.[32,33] Polarisation dependent studies have been carried out in other work to determine the direction and extent of orientation based on the relative absorption of the vibrational bands depending on the direction of polarisation of the light.[3] Using ATR-FTIR with non-polarised light in this work however eliminates the effects of the orientation dependence and means the effect can be isolated to the sensitivity to the low-temperature ferroelectric phase.

For PFM measurements, a conductive atomic force microscope (AFM) tip was used to image the surface in contact mode, while an AC voltage was applied across the sample via the tip to induce piezoelectric displacements in response to the applied field, which are then detected by the optical detector of the AFM. It allows probing of the local piezoelectric

properties of single NWs and films, and in particular, quantitative analysis of the piezo-coefficients. Furthermore, it allows for local poling of NWs and films, and extraction of the coercive voltage. [8, 19, 34, 35] PFM was used in this study to provide a direct mapping of crystalline orientation and dipole direction for both template-grown nanowires as well as films, in order to establish the self-poled nature of the nanowires that is not otherwise observed in an unpoled film.

The DSC, ATR-FTIR, permittivity, and PFM measurements were carried out on self-poled P(VDF-TrFE) nanowires grown by template wetting[25] in anodized aluminum oxide [AAO] and polyimide templates, and on P(VDF-TrFE) poled and un-poled films that were spin-caset from solution. The nanowires and films used in this study were all processed from the same solution of P(VDF-TrFE) powder in butan-2-ol, in order to maintain the same composition across all samples measured. The results were compared to determine the presence and extent of the self-poled nature of the nanowires as induced by the confinement effect of the template wetting growth process.

2. Experimental Section

2.1 Fabrication of Nanowires

P(VDF-TrFE) with co-polymer ratio 70:30 in powder form (Piezotech) was dissolved in butan-2-ol (Sigma-Aldrich) with a 1:10 ratio by weight. Nanowires were formed in either 25 mm diameter AAO (Anapore, Whatman) or 15 mm square track-etched polyimide (it4ip, Belgium) templates both with nominal pore diameters of 200 nm and of thickness 60 μm and 15 μm respectively. The fabrication process has been described in detail in Reference [25]. Figure 1(c) shows a scanning electron microscopy (SEM) image of a cross-section of a filled AAO template where the cleave has brought many of the nanowires out of the template, while Figure 1(d) shows a bundle of the nanowires in an AAO template after partially dissolving the

template with phosphoric acid. The SEM images were taken using a LEO GEMINI 1530VP microscope with an accelerating voltage of 5 kV.

2.2 Fabrication of Films

Films were fabricated using a Laurell WS-650 spin coater. The same polymer solution as used for the nanowires was pippeted onto 10 mm square ITO-coated glass substrates and a spin programme applied of 500 RPM for 10 seconds followed by 4000 RPM for 1 minute. The coated substrate was placed on a hot plate at 100 °C for ~1 hour and the process repeated twice. This method ensured no pin-holes in the film between the substrate and the top surface of the film. The end thickness of the films was determined to be ~15 μm using a surface profiler (6M, Veeco). Platinum electrodes of ~100 nm thickness were sputter-coated (k550, Emitech) onto the top surface of the films using a shadow mask. Copper wires were then attached to the top surface of the platinum film and to the ITO coating of the glass using silver conductive paint (H K Wentworth) and the films were poled by applying a potential difference of 1.1 kV between the wires using a Keithley 2410 source meter while the samples were on top of a hot plate at 100 °C. After a period of 4 hours the hot plate was turned off and the samples allowed to cool to room temperature while still applying the electric field. Following poling, ferroelectric hysteresis loops were obtained using a Radiant Technologies Precision Premier II unit at room temperature with time period of 50 ms. A hysteresis loop is shown in Figure 1(e) where the coercive field is seen to be less than the 1.1 kV over 15 μm (~73 V/ μm) applied in the poling step, demonstrating this field is sufficent for this purpose. In the cases of subsequent heat treatment the film samples were placed on a hot plate with the required temperature and time period. For PFM studies, a thinner film with nominal thickness of ~100 nm was fabricated on a 10 mm square ITO-coated glass substrate by spincoating using the same method as described for the other film samples except that, to achieve the reduced thickness, a 2% wt solution of P(VDF-TrFE) in butan-2-ol was used with a a spin

programme applied of 500 RPM for 10 seconds followed by 5000 RPM for 1 minute. The reduced thickness of the film allowed for poling to be achieved directly via the conductive AFM tip using a voltage of 10 V.

2.3 Measurements

DSC (Q2000 TA Instruments) and ATR-FTIR (Bruker Tensor 27 IR spectrometer) studies were carried out on P(VDF-TrFE) powder, small pieces of the nanowire-filled templates, and films which were carefully peeled off the substrates. Temperature-dependent permittivity measurements (4294A Impedance Analyser, Agilent Technologies) were performed on electroded nanowire-filled templates and films. PFM measurements were performed using a Bruker Multimode 8 microscope and Nanoscope V controller. Nanowires were freed from the template as described in a previous work[25] and dispersed atop a gold-coated silicon wafer, which was mounted on a standard conductive AFM holder disc, held and contacted by silver-paint. The voltages were applied to the sample, while the tip (MESP-RC-V2, Bruker) was grounded. Full details of the sample preparation and measurements are given in the Supporting Information.

3. Results and Discussion

3.1 DSC Measurements

Figure 2(a) shows DSC heating thermograms of the commercial P(VDF-TrFE) powder, P(VDF-TrFE) nanowires in AAO and polyimide templates, a poled film and films which after being poled have been subsequently heated at the indicated temperature for the indicated time. In all samples the melting peak occurs close to ~150 °C while the lower temperature peaks correspond to the ferroelectric Curie transition. The poled film is seen to have a Curie temperature of ~105°C which for the sample heated at 100°C for 2 hours moves to ~111°C and for the sample heated at 135°C moves to ~94°C. These effects when heating

above and just below the Curie temperature are in good agreement with the effects reported by Ohigashi et al.[31] where, in comparison with the initially poled sample taken to have large domains, the samples with a peak shifted to lower temperatures were inferred to have small domains and the samples with a peak shifted to higher temperatures were inferred to have medium sized domains intermediate between the initial sample and the samples with a shift to lower temperatures. In this work the transitions all occur at lower temperatures which is expected because of the lower ratio of VDF:TrFE in the copolymer used.[15,36] Our observed shift in melting temperature of the films when annealed below and above the Curie temperature is also consistent with previous reports on where a similar effect is observed in P(VDF-TrFE) (75:25 mol%) films.[37]

Heating the poled films at 135 °C and 105 °C are therfore taken to progressively create regions of small and medium domains respectively until the entirety of the material is converted. In both cases intermediate traces are seen with multiple peaks broadening the entire transition when heating at these temperatures for shorter times, which is taken to indicate the presence of different domain size regions. The powder is seen to have a transition temperature close to that of the film which is de-poled as a result of the heating at 135 °C, while the nanowire-filled AAO template sample is seen to have a Curie transition temperature matching that of the poled film, thus pointing towards the similar crystalline nature of the nanowires with the low-temperature phase structure, resulting from the nano-confinement effect. The nanowire filled polyimide template sample has a broader transition centred at ~109 °C which may be an indication of a broader range in domain size with more gauche defects resulting in some smaller domain sizes than in the poled film and AAO template nanowire filled sample.

The enthalpy per gram (the net mass of P(VDF-TrFE) is used in the cases of template filled samples) associated with both the ferroelectric to paraelectric transition (H_c) and the melting transition (H_m) are found to be highest for the nanowire-filled AAO sample followed

respectively by the nanowire-filled polyimide sample, poled film, the film heated at 100 °C, the film heated at 135 °C and lastly the powder, as shown in Table 1. This indicates that the template-grown nanowires have the highest overall crystallinity followed by the samples in the same order as the enthalpy values. Quantitative values of crystallinity can be calculated for PVDF based on the enthalpy of the melting transition compared with the known enthalpy of fusion for completely crystalline PVDF. Similar calculations have been carried out in other work for PVDF co-polymers,[38-41] but this presents difficulties which are not taken into account as the value of the enthalpy of fusion is estimated from that of PVDF where there is no prior ferroelectric to paraelectric transition before melting, whereas with P(VDF-TrFE) the desired value of crystallinity is that preceding the ferroelectric to paraelectric transition.[42] For P(VDF-TrFE), various values of the enthalpy of fusion have been used without agreement even for the same copolymer compositions and have been calculated either using the enthalpy associated with the melting transition or that combined with the enthalpy associated with the ferroelectric to paraelectric transition.[42] The enthalpy values therefore remain able to give a quantitative comparison of crystallinity but absolute values of crystallinity are not asserted.

3.2 ATR-FTIR Measurements

Figure 2(b) shows ATR-FTIR traces of the nanowire-filled AAO template, powder and film samples as for the DSC data with the data presented for the films heated at 100 °C and 135 °C being those heated for 2 hours and 4 hours respectively as this showed a complete transformation to a DSC thermogram trace with a single transition corresponding to a different crystalline regime. The nanowire-filled AAO template trace is shown after subtraction of a scaled bare AAO template trace. The nanowire-filled polyimide template is omitted because of similarity in spectral positions of bands for a bare polyimide template (see supplementary information).

The data is presented normalised from the background complete transmission to the depth of the ~880 cm^{-1} trough. The bottom left inset shows an enlarged view around the ~880 cm^{-1} and ~840 cm^{-1} bands where the data is shifted to intersect at the ~880 cm^{-1} trough such that a comparison in the depth of the ~880 cm^{-1} and ~840 cm^{-1} depth can be visibly made. The value of the ~840 cm^{-1} trough depth relative to the the ~880 cm^{-1} trough, f_{840}/f_{880}, is highest for the template-grown nanowire sample followed by the poled film sample both of which are greater than 1. The values then decrease for the film heated to 100 °C, the film heated to 135 °C and the powder sample in this respective order all of which are lower than 1. This matches the same trend as for the DSC enthalpy data (see Table 1).

3.3 Permittivity Measurements

Figure 3 shows permittivity against temperature data for a nanowire-filled AAO template sample (Figure 3a), a nanowire-filled polyimide template sample (Figure 3b), poled film (Figure 3c) and an un-poled film (Figure 3d). Figure 3(e) shows permittivity against temperature data for a poled film which is subsequently cyclically heated to 135°C for 20 minutes. In Figure 3(a)-(d) data is presented at frequencies of 500 Hz, 1 kHz, 5 kHz, 10 kHz, 50 kHz and 100 kHz. In figure 3(e) data is limited to 50 kHz for visual clarity. In all cases the relative permittivity increases with increasing temperature as the polymer approaches the Curie transition and the fixed nature of the polarisation associated with the ferroelectric behaviour of the material is weakened. A peak in permittivity occurs at the Curie transition and following this the permittivity decreases with increasing temperature under the effects of increased thermal energy on the now paraelectric material.

The ferroelectric to paraelectric transition for the nanowire-filled AAO sample and poled film is seen to occur with a peak at ~105 °C and the transition for the nanowire-filled polyimide template sample is at 108 °C. In the cooling traces hysteresis is seen and the reverse paraelectric to ferroelectric transition is seen to occur at ~71 °C, ~73 °C and ~75 °C

respectively for the AAO, poled film and polyimide samples. The permittivity values for the nanowire samples are seen to have a broader variation with frequency but relatively similar overall values of permittivity throughout the heating cycles as compared to the poled film.

For the unpoled film the ferroelectric to paraelectric transition is seen to occur centred at 97°C which is in reasonable agreement with the poled film that is subsequently heated to 135°C in the DSC measurements. The values of permittivity are seen to be notably higher than for the nanowire and poled film data during the heating cycle. In Figure 3(e) the result of heating a poled film at 135 °C is seen to increasingly broaden the transition in the heating stage and shift it to lower temperature. In the cooling stage there is also a shift to lower temperature of the reverse transition and a lip is seen to become present on the lower temperature side of the transition. Similar trends for permittivity against temperature traces when heating above the Curie point have been previously reported for poled films of P(VDF-TrFE)[43,44] and the trend is in agreement with the differences between the poled and unpoled film data. A similar process of measurement after successive heating steps on an unpoled film did not show a shift in the transition temperature (see Supporting information), which further verifies that the shift in temperature seen when heating the poled film to be a result of removing the orientation of the film and the conversion to a structure characteristic of the cooled phase.

3.4 PFM Measurements

Figure 4 shows PFM measurements taken on an unpoled film with nominal thickness of 100 nm (see Supporting information S5) and on as-grown nanowires that have been freed from the template by dissolving it in phosphoric acid, and dispersed on a conducting gold-coated Si substrate. In addition to topographic data, the in-phase signal (X channel) of the cantilever's vertical displacement was used to quantify the piezo-response of both the film and the nanowires. Measurement on Bruker's *PFM-SMPL* $LiNbO_3$ calibration sample was

carried out prior to each set of PFM measurements in order to calibrate the deflection sensitivity[45] (see Supporting Information S5 for details of the calibration procedure).

Figures 4(a) and (b) respectively show the height and PFM images of the unpoled film, with a central poled region where a DC offset electric field has been applied, as can be seen in the brighter region of Figure 4(b). The effective piezoelectric coefficient (d_{33}) was found to be 17.5 pm/V in the poled region, while the unpoled regions had an average d_{33} value of -1.2 pm/V which was within the noise limit as observed on bare Si (+/- 2 pm/V). Figures 4(c) and (d) show the height and PFM data taken on a set of three nanowires before a voltage bias is applied across the central region, while Figures 4(e) and (f) show the height and PFM images of the same area after poling of the central region through application of a 10 V voltage bias. The self-poled nature of the nanowires is evident in the PFM images as a clear piezoresponse signal (9.4 pm/V) is obtained from the nanowires even without the application of a voltage as can be clearly seen in Figure 4(d), which is absent in the unpoled portion of the film in Figure 4(b). Upon application of a voltage bias across the central region in a direction perpendicular to the long axis of the nanowires, the piezoresponse signal increases in magnitude to 19.9 pm/V. This increase in the piezoresponse signal indicates re-orientation of dipoles which were originally along the long axis of the nanowire (31 mode) to an orientation perpendicular to the long axis of the nanowire (33 mode). Our PFM results thus indicate that the nanowires are self-poled and that the net orientation of the dipoles is along the long axis of the nanowire. This is consistent with our previous reported work[25] where a piezoelectric output voltage is obtained when vertically aligned nanowire-filled templates are subjected to a periodic compressive force along their lengths. Furthermore, we show in Supporting Information S4 that a poled film generates a piezoelectric output signal when subjected to periodic impacting (Figures S4-1 and S4-2), similar to what is observed in nanowire-filled template samples (Figures S4-5 to S4-8), whereas unpoled films show no net piezoelectric output signal under similar mechanical excitation (Figures S4-3 and S4-4).

4. Conclusions

Figure 5 shows trends across the characterization results. The similarities observed in the physical properties of the template-grown nanowires and poled films, in conjunction with the PFM results, clearly indicate the self-poled nature of the nanowires, as induced by the confined template-assisted growth process. This fabrication process thus results in an aligned all-trans structure characteristic of the low-temperature phase in the as-grown nanowires. The f_{840}/f_{880} and enthalpy values of the AAO templated nanowires both being greater than the poled film indicate a higher degree of crystallinity with less defects. As the trend in enthalpy matches that of the f_{840}/f_{880} values across all the samples, this provides verification for the validity of these measurements. The nanowires fabricated in polyimide templates are seen to also have high enthalpy values, close to the poled film, indicating a high crystallinity, though the slight increase in Curie temperature is indicative of the presence of some gauche defects. The difference in results for nanowires fabricated in AAO and polyimide templates may arise from difference in hydrophobicity and flexibility of the templates. The mechanism for the observed preferential crystallisation behaviour has been linked to preferential nucleation and growth from the pore walls after precursor wetting leads to a thin film coating the surface of the pores prior to complete filling.[18,24] Previous work has corroborated that this results in crystallisation into the all trans phase with the polar b axis orientated parallel to the nanowire length with crystalline lamella stacked perpendicular to this.[17,18,24] It has also been shown that crystallisation with the a axis orientated parallel to the nanowire length is possible, providing the required experimental conditions and in particular necessary thermal treatment has been applied.[19] Recently the polarity of the solvent and hydrophobic nature of the pore walls have also been explored as effects contributing to the mechanism responsible for enhancement of the all trans phase.[26] In the case of AAO templates, hydroxyl groups terminate the pore walls and these may restrict rotation in the polymer as a result of hydrogen bond interactions between these

hydroxyl groups and the fluorine atoms of PVDF and P(VDF-TrFE). It was recently shown that treating templates to maximise this effect can result in similar confinement and preferential crystallisation for the homopolymer PVDF as well as P(VDF-TrFE),[26] which again results in piezoelectric behaviour without poling, as observed in our template-grown nanowires. Thus, the quantitative results presented in this paper allow the means for comparison with future reported P(VDF-TrFE) nanostructures and determination of the existence of their self-poled nature. Additionally, the higher ferroelectric crystalline quality observed for the template-grown nanowires is in strong agreement with previous reports of enhanced piezoelectric properties.

Supporting Information

Supporting Information is available from the Wiley Online Library or from the author

Appendix/Nomenclature/Abbreviations

Acknowledgements: The authors are grateful for financial support from the European Research Council through an ERC Starting Grant (Grant no. ERC-2014-STG-639526, NANOGEN). R.A.W. thanks the EPSRC Cambridge NanoDTC, EP/G037221/1, for studentship funding.

Received: Month XX, XXXX; Revised: Month XX, XXXX; Published online:
((For PPP, use "Accepted: Month XX, XXXX" instead of "Published online")); DOI: 10.1002/marc.((insert number)) ((or ppap., mabi., macp., mame., mren., mats.))

Keywords: ferroelectric, nanowire, polymer, self-poling, template-wetting

[1] A. J. Lovinger, *Science*, **1983**, 220, 1115.

[2] S. Crossley, S. Kar-Narayan, *Nanotechnology*, **2015**, 26, 344001.

[3] S. Crossley, R. A. Whiter and S. Kar-Narayan, *Mater. Sci. Technol*., **2014**, 30, 1613.

[4] D. Mandal, S.Yoon, K. J. Kim, *Macromol. Rapid Commun.*, **2011**, 32, 831.

[5] O. Pabst, S. Hölzer, E. Beckert, J. Perelaer, U. S. Schubert, R. Eberhardt, A. Tünnermann, *Organic Electronics*, **2014**, 15, 3306.

[6] Z. Hu, M. Tian, B. Nysten, A. M. Jonas, *Nature Materials*, **2009**, 8, 62.

[7] R. Cai, H. G. Kassa, R. Haouari, A. Marrani, Y. H. Geerts, C. Ruzié, A. J. J. M. van Breemen, G. H. Gelinck, B. Nysten, Z. Huf, A. M. Jonas, *Nanoscale*, **2016**, 8, 5968,

[8] R. Cai, H. G. Kassa, A. Marrani, A. J. J. M. van Breemen, G. H. Gelinck, B. Nysten, Z. Hu, A.M. Jonas, *Appl. Phys. Lett*., **2014**, 105, 113113

[9] R. Hasegawa, Y. Takahashi, Y. Chatani, H. Tadokoro, *Polym. J.* **1972**, 3, 600.

[10] T. Furukawa, *Phase Transit.* **1989**, 18, 143.

[11] K. Nakamura, Y. J. Wada, *Polym. Sci.*, **1971**, 9, 161.

[12] F. Micheron, *Rev. Tech. Thomson-CSF*, **1979**, 11, 513.

[13] Y. Higashihata, J. Sako, T. Yagi, *Ferroelectrics*, **1981**, 32, 85.

[14] A. J. Lovinger, T. Furukawa, G. T. Davies, M. G. Broadhurst, *Polymer*, **1983**, 24, 1233.

[15] R. Gregorio, M. M. Botta, *J. Polym. Sci. Pol. Phys.*, **1998**, 36, 403.

[16] K. Tashiro, R. Tanaka, *Polymer*, **2006**, 47, 5433.

[17] J. L. Lutkenhaus, K. McEnnis, A. Serghei, T. P. Russell, *Macromolecules*, **2010**, 43, 3844.

[18] V. Cauda, S. Stassi, K. Bejtka, G. Canavese, *ACS Appl. Mater. Interface*, **2013**, 5, 6430.

[19] Y. Wu, Q. Gu, G. Ding, F. Tong, Z. Hu, A. M. Jonas, *ACS Macro Lett*., **2013**, 2, 535.

[20] D. Guo, N. Setter, *Macromolecules*, **2013**, 46, 8569.

[21] V. Cauda, B. Torre, A. Falqui, G. Canavese, S. Stassi, T. Bein, M. Pizzi, *Chem. Mater.* **2012**, 24, 4215.

[22] C.-C. Hong, S.-Y. Huang, J. Shieh, S.-H. Chen, *Macromolecules*, **2012**, 45, 1580.

[23] M.-C. Garcia-Gutierrez, A. Linares, J. J. Hernandez, D. R. Rueda, T. A. Ezquerra, P. Poza, R. J. Davies, *Nano Lett.*, **2010**, 10, 1472.

[24] W. H. Liew, M. S. Mirshekarloo, S. Chen, K. Yao, F. E. H. Tay, *Sci. Rep., **2015**, 5, 9790.*

[25] R. A. Whiter, V. Narayan, S. Kar-Narayan, *Adv. Energy Mater*., **2014**, 4, 1614.

[26] C. Fu and X. Wang and X. Shi and X. Ran, *RSC Adv*., **2015**, 5, 87429

[27] J. Chang, M. Dommer, C. Chang, L. Lin, *Nano Energy*, 2012, 1, 356.

[28] J. Song, H. Lu, S. Li, L. Tan, A. Gruverman, S. Ducharme, *Nanotechnology*, **2016**, 27, 015302.

[29] K. Tashiro, K. Takano, M. Kobayashi, Y. Chatani, H. Tadokoro, *Polymer*, **1984**, 25, 195.

[30] K. Tashiro, M. Kobayashi, *Polymer*, **1986**, 27, 667.

[31] H. Ohigashi, N. Kagami, G. R. Li, *J. Appl. Phys*., **1992**, 71, 506.

[32] K.J. Kim, N.M. Reynolds, S.L. Hsu, *Macromolecules*, **1989**, 22, 4395.

[33] K. Tashiro, M. Kobayashi, *Spectrochim. Acta.*, **1994**, 50A, 1573.

[34] V. Sencadas, C. Ribeiro, I. K. Bdikin, A. L. Kholkin, and S. Lanceros-Mendez, *Phys. Status Solidi A*, **2012**, 209, 12.

[35] P. Sharma, D. Wu, S. Poddar, T. J. Reece, S. Ducharme, A. Gruverman, *J. Appl. Phys.* , **2011**, 052010.

[36] K. Tashiro, K. Takano, M. Kobayashi, Y. Chatani, H. Tadokoro, *Ferroelectrics*, **1984**, 57, 297.

[37] M. A. Barique, H. Ohigashi, Polymer, 2001, 42, 4981.

[38] H. Kodama, Y. Takahashi, T. Furukawa, *Ferroelectrics*, **1997**, 203, 433.

[39] P. Cebe and J. Runt, *Polymer*, **2004**, 45, 1923.

[40] J. Clements, G. R. Davies, I. M. Wardt, *Polymer*, **1992**, 33, 1623.

[41] G. S. Buckley, C. M. Roland, R. Casalini, A. Petchsuk, T. C. Chung, *Chem. Mater.* **2002**, *14*, 2590.

[42] G. Teyssèdre, C. Lacabanne, *Ferroelectrics*, **1995**, 171, 125.

[43] K. Urayama, M. Tsuji, D. Neher, *Macromolecules*, **2000**, 33, 8269.

[44] J. F. Legrand, *Ferroelectrics*, **1989**, 91, 303.

[45] T. Jungk, Á. Hoffmann, E. Soergel, *Journal of Microscopy*, **2007**, 227, 1.

Figure 1. {(a) and (b) show the chain structure of P(VDF-TrFE) in the low-temperature and cooled phases respectively. The inset in (b) shows a rotation around the chains such that the chain direction is more easily observed. (c) Scanning electron microscopy images of (left) a cross-section of a nanowire filled AAO template where the cleave has removed a number of nanowires out of the pores. In the right image a bundle of the nanowires are seen after partially etching away the template. (d) Ferroelectric hysteresis loop taken on a film of P(VDF-TrFE)}

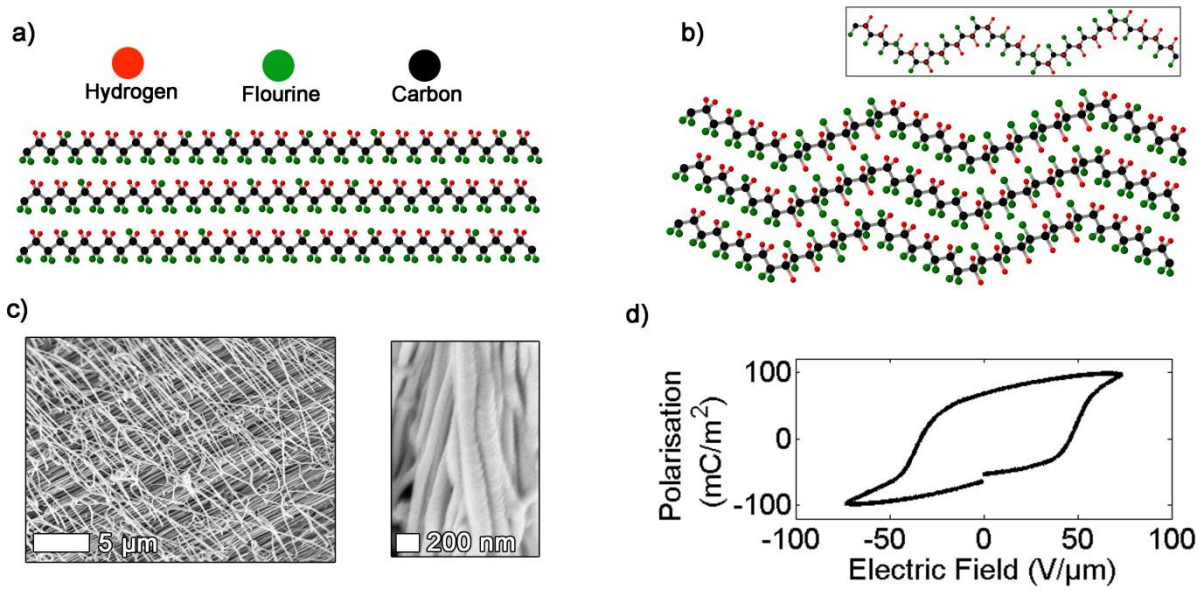

Figure 2. {(a) DSC heating thermograms and (b) ATR-FTIR spectra of P(VDF-TrFE) nanowire-filled AAO and polyimide templates, as well as spin-coated films of P(VDF-TrFE) after poling and after subsequent heating at the indicated temperature for the indicated time. The bottom right plot of (b) shows an enlarged view of the ATR-FTIR results in the region of the 840 cm^{-1} and 880^{-1} troughs.}

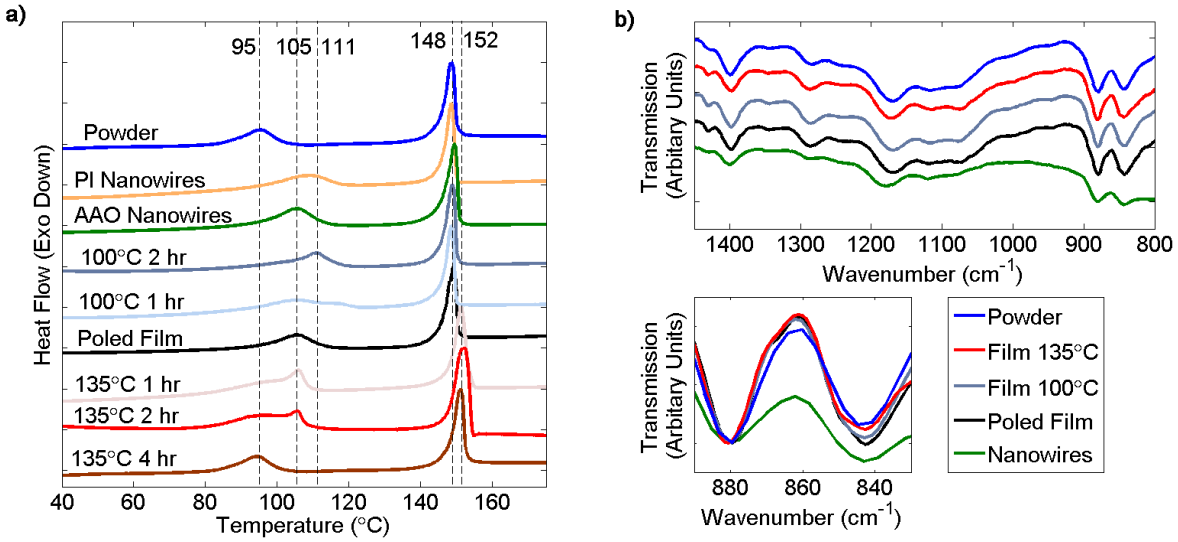

Figure 3. {Dielectric permittivity versus temperature plots at the indicated frequencies for (a) nanowires inside AAO templates, (b) nanowires inside polyimide templates, (c) a poled film of P(VDF-TrFE) and (d) an unpoled film of P(VDF-TrFE). (e) Dielectric permittivity versus temperature at 50 kHz of an initially poled film, before and after being subjected to successive de-poling heating steps.}

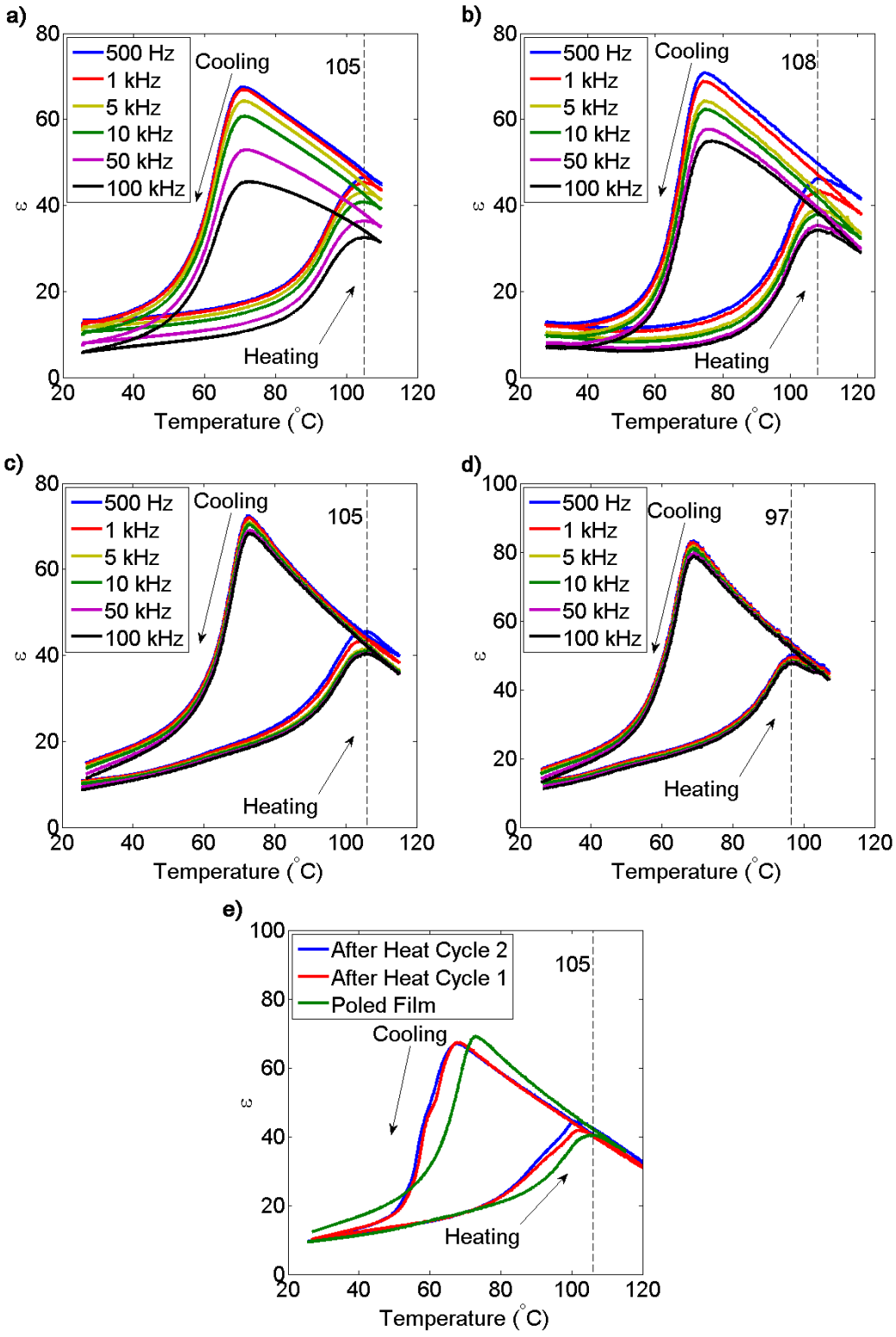

Figure 4. {Scanning probe studies on P(VDF-TrFE) film and nanowire samples. (a-b) Height and PFM images of film sample with a central poled region of ~2.5 × 1.5 μm over which a DC offset field has been applied. (c-d) Height and PFM images of nanowire sample prior to application of DC bias. (e-f) Height and PFM images of nanowire sample after a DC offset field has been applied over a central region of width ~2.5 μm, the middle of the vertical axis matches that of (c-d). (g-h) In-phase signal hysteresis loops for poled film and nanowire regions when ramping with a DC offset field between +/-10 V. In all cases the PFM images were measured using an AC voltage of 2 V.}

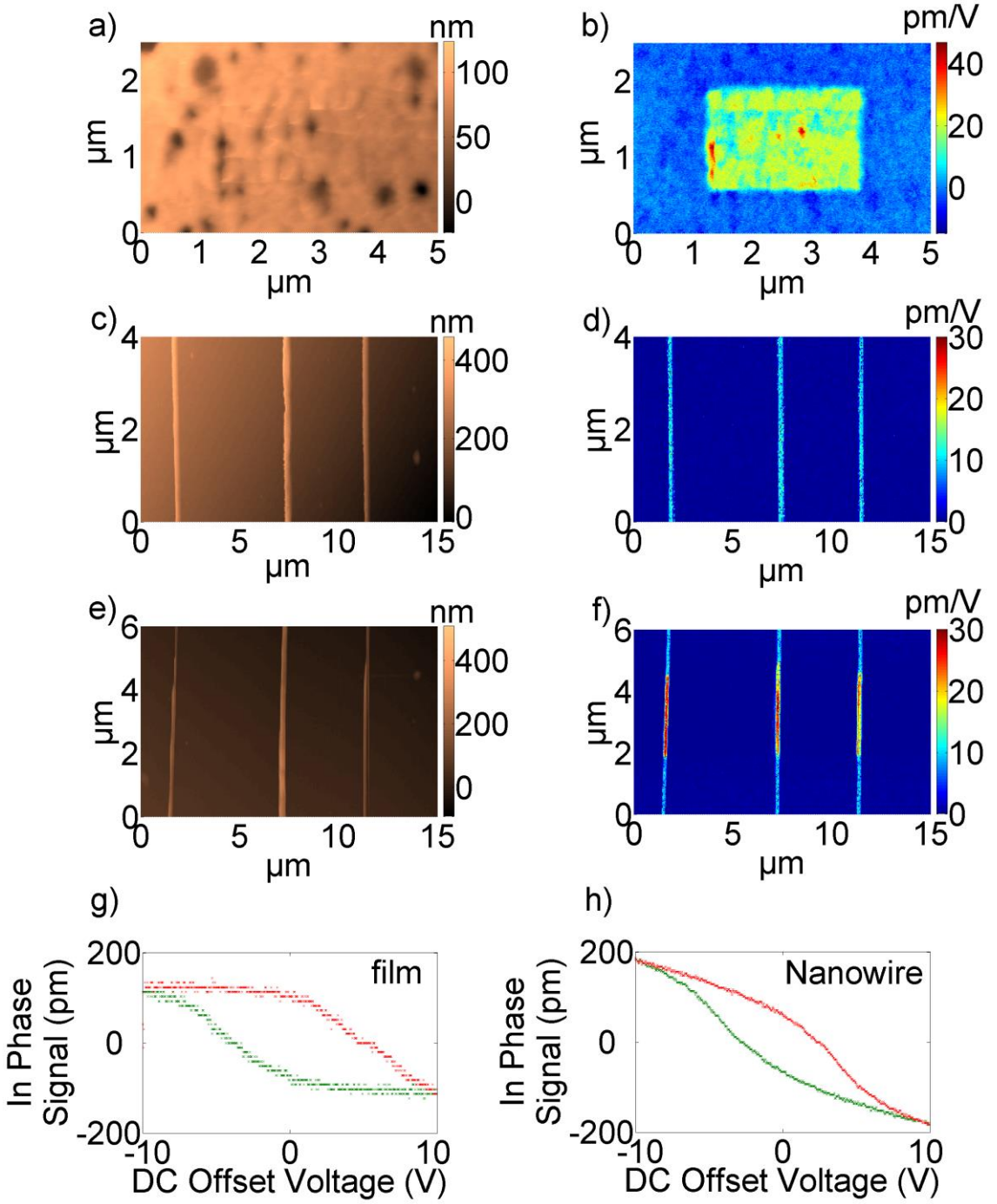

Figure 5. {Plots of trends of Curie temperature, f_{840}/f_{880} and the sum of the enthalpy per gram of the ferroelectric to paraelectric phase transition. The abbreviations that label the data points are given in Table 1.}

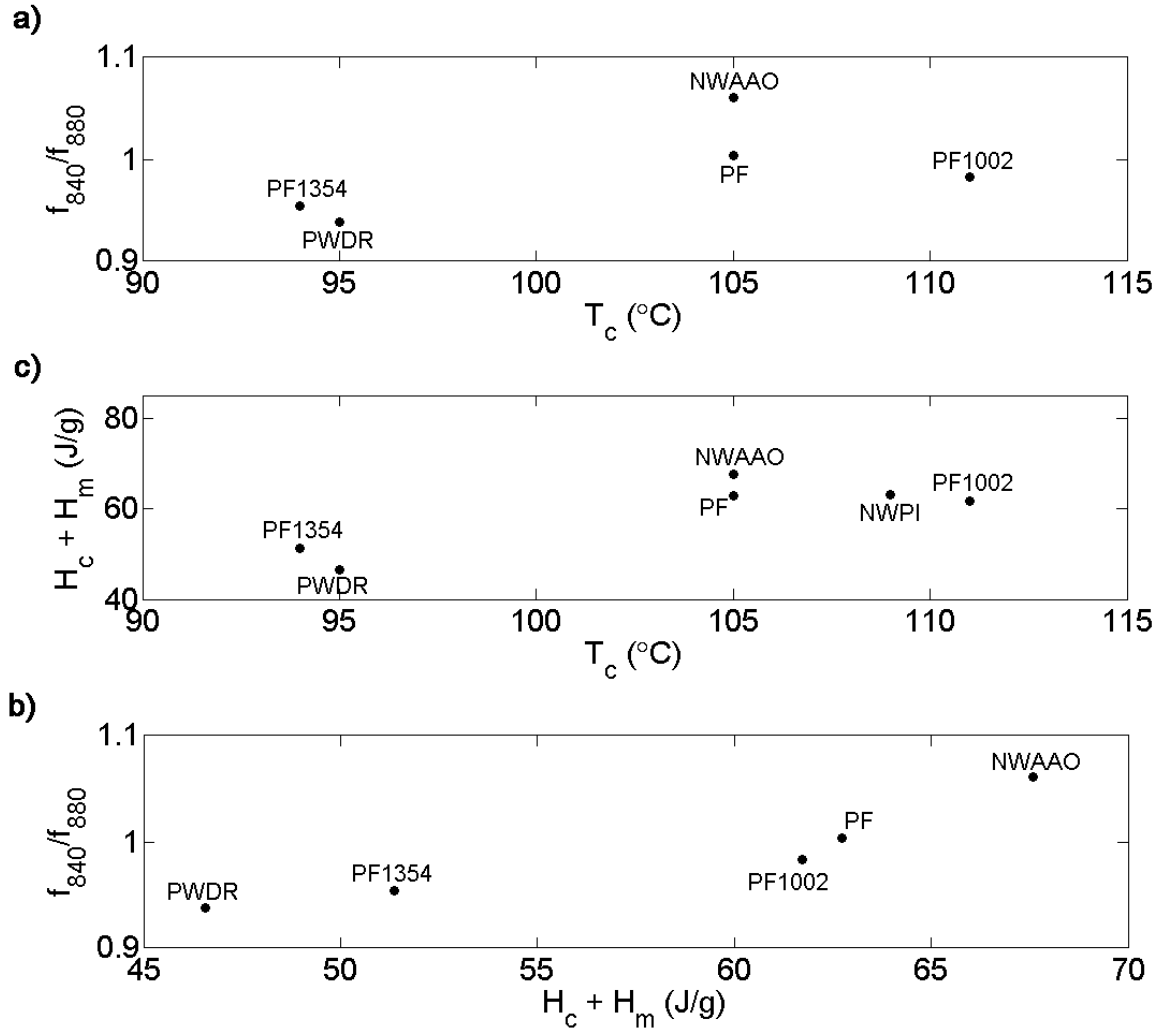

Table 1. {Metrics of characterization methods carried out on the indicated samples of P(VDF-TrFE) nanowires and films.}

Sample	**Abbreviation**	**f_{840}/f_{880}**	**T_C [°C]**	**H_c [J/g]**	**H_m [J/g]**
Nanowires in AAO template	NWAAO	1.06	105	28.8	38.8
Nanowires in polyimide template	NWPI	-	108	26.4	36.7
Poled Film	PF	1.00	105	26.6	36.18
Poled Film heated at 100 °C for 2 hours	PF1002	0.98	111	25.9	35.86
Poled Film heated at 135 °C for 4 hours	PF1354	0.95	94	17.4	33.99
Powder	PWDR	0.94	95	17.1	29.49

“Self-poled” polyvinylidene-fluoride (P(VDF-TrFE)) nanowires fabricated by solution wetting of nanoporous templates are measured with differential scanning calorimetry, Fourier transform IR spectroscopy and dielectric permittivity measurements. These are quantitatively compared with measurements taken on electrically poled spin-coated films before and after subsequent de-poling heat treatment to observe trends and determine the extent and nature of the self-poling effect in the nanowires as induced by the confined growth process.

R. A. Whiter, Y. Calahorra, C. Ou, S. Kar-Narayan*

Observation of Confinement-induced Self-Poling Effects in Ferroelectric Polymer Nanowires grown by Template Wetting

ToC figure ((Please choose one size: 55 mm wide × 50 mm high **or** 110 mm wide × 20 mm high. Please do not use any other dimensions.))

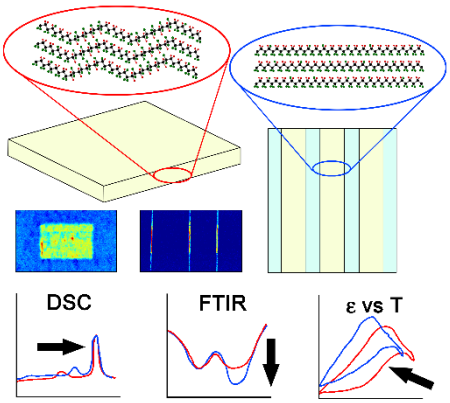

((Supporting Information should be included here for submission only; for publication, please provide Supporting Information as a separate PDF file.))

Supporting Information

for *Macromol. Rapid Commun.*, DOI: 10.1002/marc.2013#####

1. Sample preparation and measurements

1.1 DSC

DSC measurements (Q2000 TA Instruments) were carried out on P(VDF-TrFE) powder, small pieces of the nanowire-filled templates, and films which were carefully peeled off the substrates using tweezers, each with a sample mass of ~3 mg. DSC measurements were carried out using heating and cooling rates of 10 °C/minute and equilibrium established at 25 °C prior to each measurement.

1.2 ATR-FTIR

ATR-FTIR measurements (Bruker Tensor 27 IR spectrometer) were carried out on samples as prepared for DSC above. Following a baseline measurement the samples were placed on an IR transparent high refractive index crystal on which the IR beam is incident and pressure was applied from a small metal disk to ensure contact between the sample and the crystal. IR spectograms were generated with an average of 16 spectra taken for each measurement.

1.3 Dielectric Permittivity versus Temperature

For dielectric permittivity versus temperature measurements the nanowire-filled templates had platinum electrodes of ~100 nm thickness sputter coated (k550, Emitech) onto either side and copper wires attached with silver conductive paint. The templates were then mounted between glass slides for measurement. The films were measured while remaining on the ITO substrates

using the same electrodes as for poling. When measuring, a sample was placed on a copper block housing heating elements and a PT100 thermometer, all sealed in a nitrogen enviroment. Heating and cooling was controlled at 1 °C/minute (336, Lakeshore termperature controller) and permitivity measurements were continously taken between frequencies of 500 Hz and 100 kHz using an impedance analyser (4294A, Agilent Technologies). Dielectric permittivity values for P(VDF-TrFE) structures were obtained from measured capacitances based on measured or known sample geometry.

2. ATR-FTIR measurements of nanowire-filled polyimide templates.

ATR-FTIR measurements of empty and nanowire filled polyimide template. The significant overlap of bands, particularly at 880 cm^{-1} meant that an accurate extraction of data indicative of just the nanowires was judged not to be able to be suitably achieved.

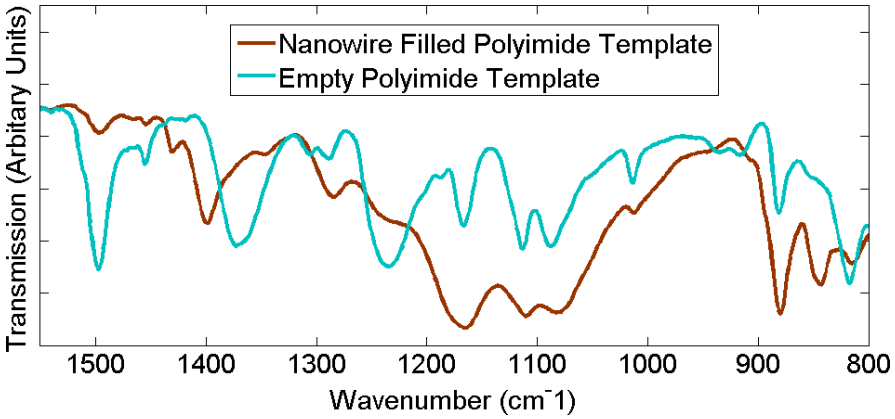

3. Dielectric permittivity data for un-poled P(VDF-TrFE) film

Dielectric permittivity against temperature data for an un-poled film of P(VDF-TrFE) which subsequently goes cycles of being heated to 135°C for 20 minutes. No discernable shift in the Curie temperature is observed. After the first heat cycle the permittivity has a slight increases but this is not repeated after a second heat cycle. This indicates fully depoled P(VDF-TrFE)

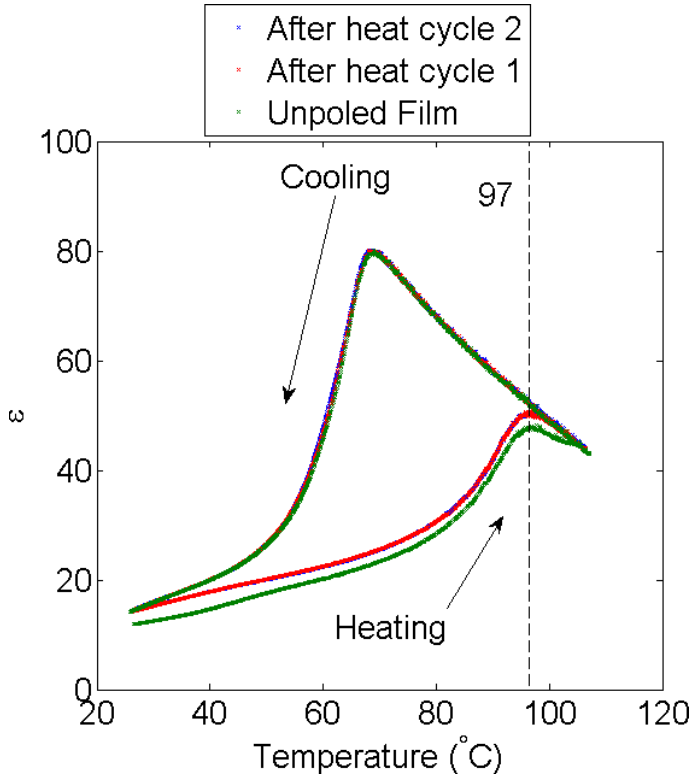

4. Piezoelectric Response Impact Measurements

A piezoelectric response was measured by impacting samples with an aluminium disk attached to the oscillating arm of a permenant magnetic shaker (LDS Systems V100) at a frequency of 5 Hz. Electrodes were applied as described for the permittivity measurements. Nanowire-filled template samples were impacted along the length of the nanowires and film samples along the film thickness. Open circuit voltage and closed circuit current measurements were taken independently with further description of the measurement set-up described previously in Reference [1].

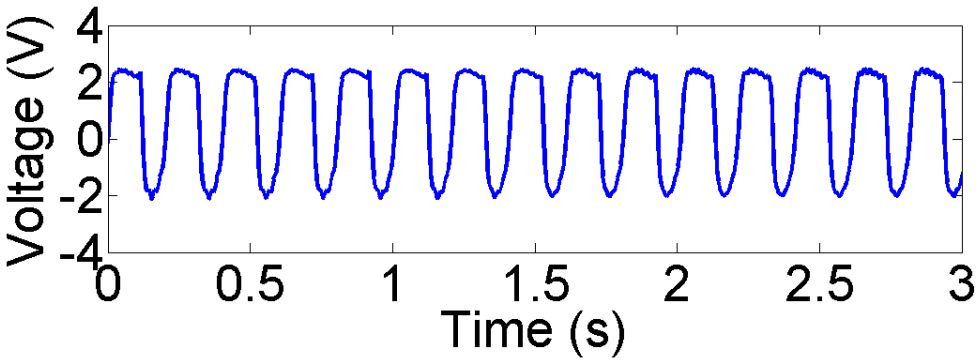

Figure S4-1: Open circuit voltage for poled film

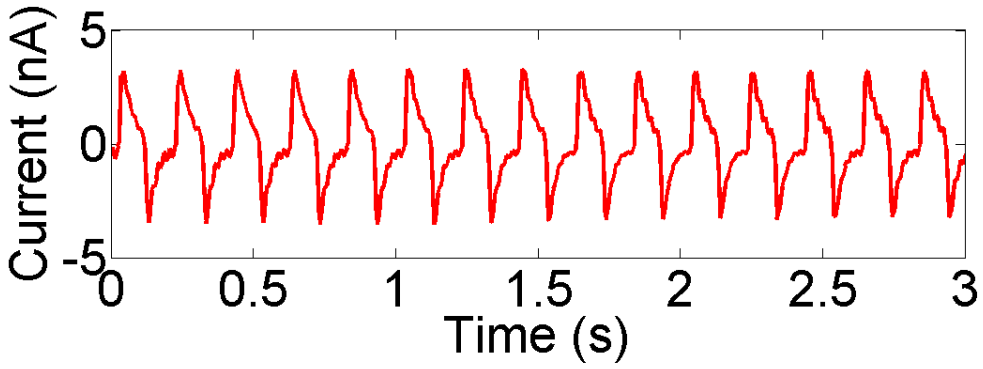

Figure S4-2: Closed circuit current for poled film

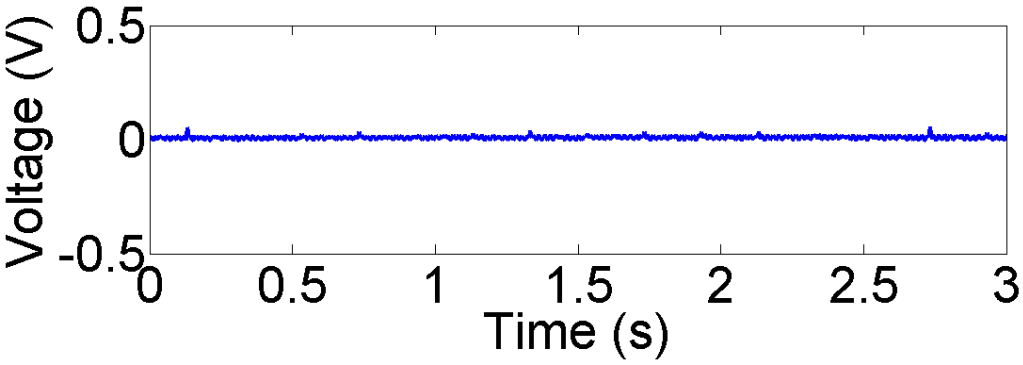

Figure S4-3: Open circuit voltage for unpoled film

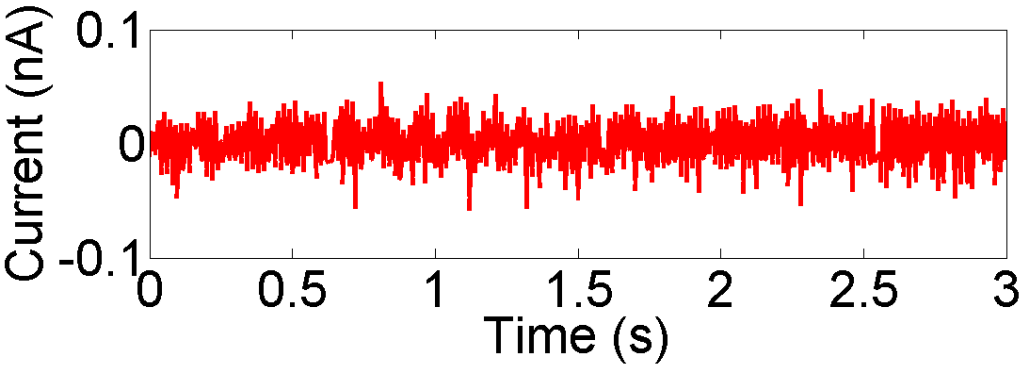

Figure S4-4: Closed circuit current for unpoled film

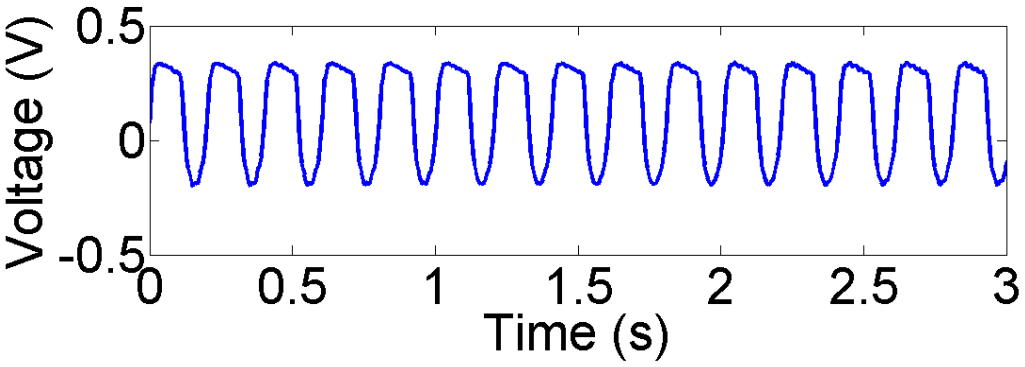

Figure S4-5: Open circuit voltage for nanowire filled polyimide template

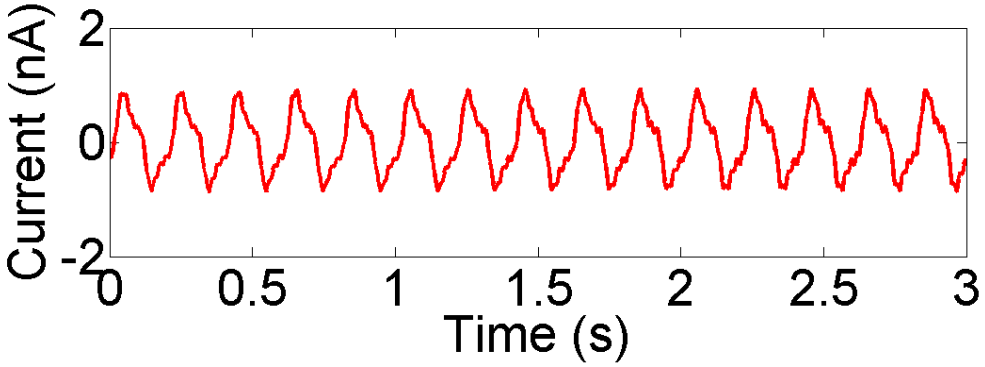

Figure S4-6: Closed circuit current for nanowire filled polyimide template

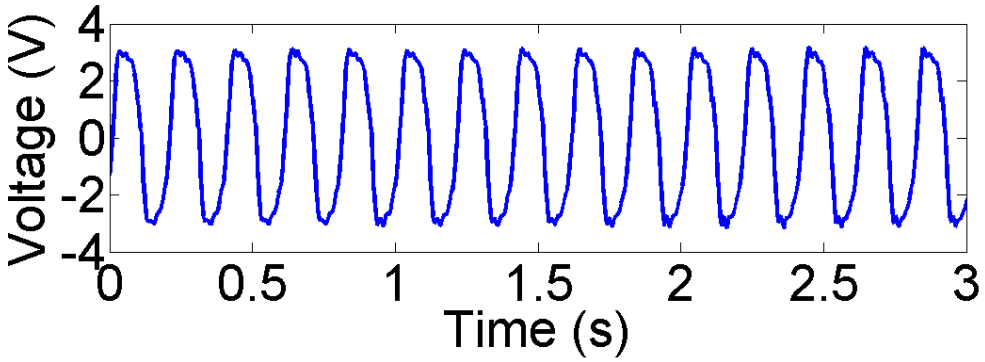

Figure S4-7: Open circuit voltage for nanowire filled alumina template

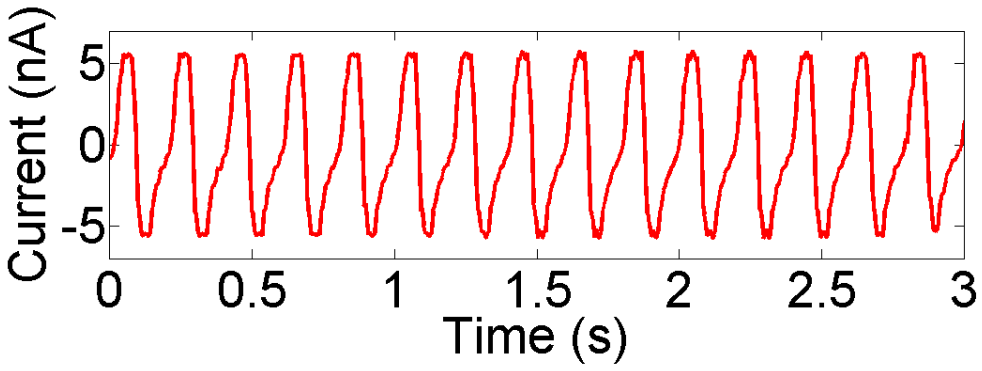

Figure S4-8: Closed circuit current for nanowire filled alumina template

5. PFM Measurements

5.1 Preparation of Film

A film with nominal thickness of ~100 nm for PFM measurements was fabricated on a 10 mm square ITO-coated glass substrate by spincoating using the same method as described for the other film samples except that, to achieve the reduced thickness, a 2% wt solution of P(VDF-TrFE) in butan-2-ol was used with a a spin programme applied of 500 RPM for 10 seconds followed by 5000 RPM for 1 minute.

5.2 Calibration Sample

Measurement on Bruker's *PFM-SMPL* $LiNbO_3$ calibration sample was carried out prior to each set of PFM measurements in order to calibrate the deflection sensitivity. A PFM image of the striped $LiNbO_3$ sample for calibration is shown in Figure S5-1. To perform the calibration a shift was performed so as to bring the mid-point of the positive and negative striped region signals to 0. A scaling was then performed so as to set the shifted signal of the positive and negative striped regions to +/-7.5 pm/V. That is to say the following transformation was applied to convert an original data point, D_o, in volts to a calibrated data point, D_c, in pm where C_p and C_n are the average in phase signal of alternating striped regions

of the calibration sample in volts and V_{ac} is the applied AC driving voltage, also in volts used to acquire the calibration sample PFM image. For the PFM images of nanowires and films as well as the calibration sample the value of V_{ac} used was 2 V at 200 kHz. Poling was achieved by applying a DC offset potential of -10 V during a scan over a specified region.

$$D_c=[D_o - C_p + (C_p - C_n)/2)]/[(C_p - C_n)/2]*7.5*V_{ac}$$

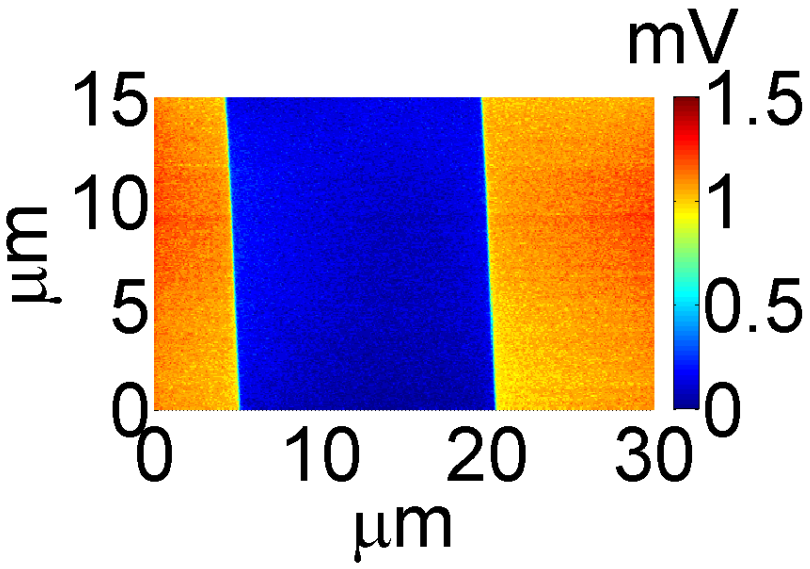

Figure S5-1: PFM Image of calibration sample

5.3 Regions of Measurement

For determining d_{33} values for nanowires and the film, averages were taken over the regions shown in black. For the film the left region is for the unpoled value and the right region is for the poled value.

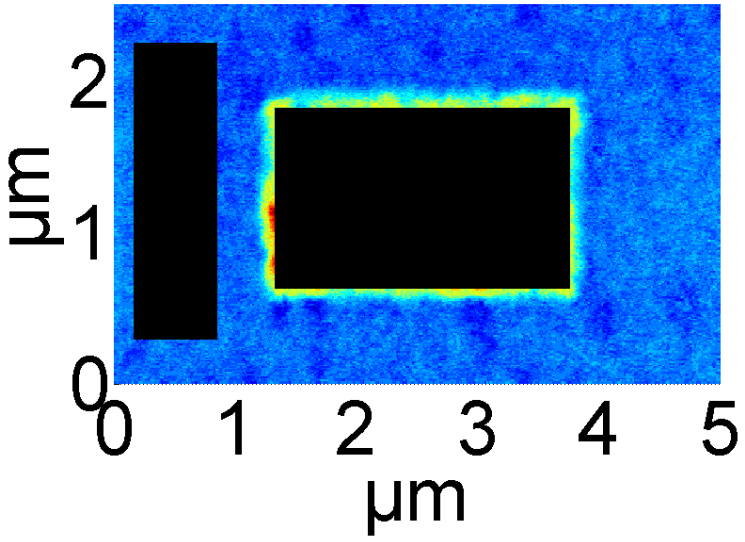

Figure S5-2: Regions of measurement for film

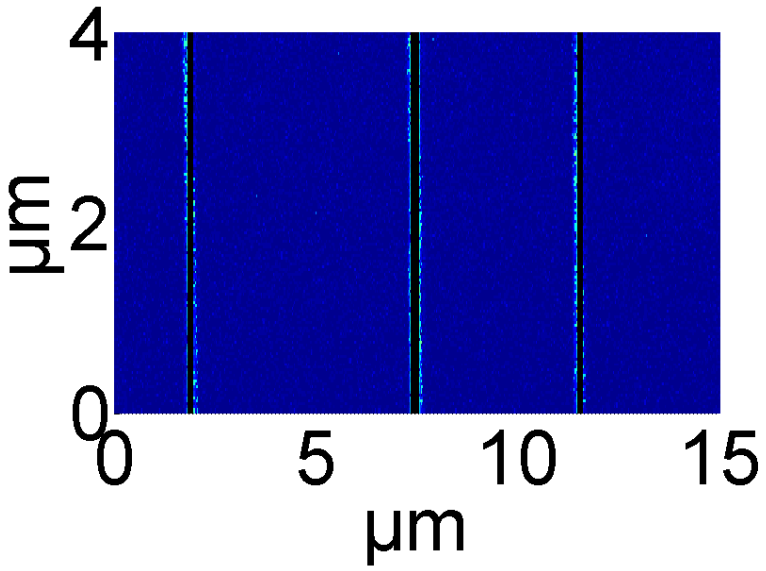

Figure S5-3: Region of measurement for nanowires prior to poling

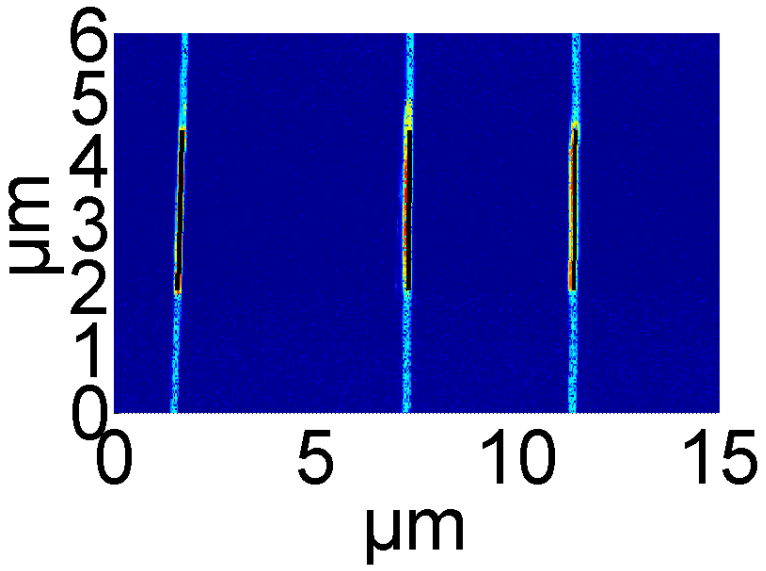

Figure S5-4: Region of measurement for nanowires after poling

[1] *R. A. Whiter, V. Narayan, S. Kar-Narayan, Adv. Energy Mater.*, ***2014***, *4, 1614.*

Observation of Confinement-induced Self-Poling Effects in Ferroelectric Polymer Nanowires grown by Template Wetting

R. A. Whiter, Y. Calahorra, C. Ou, S. Kar-Narayan*